

Optimization of Gating System Design for Die Casting of Thin Magnesium Alloy-Based Multi-Cavity LCD Housings

B.D. Lee, U.H. Baek, and J.W. Han

(Submitted April 18, 2011; in revised form November 30, 2011)

High-pressure die casting is the preferred process for manufacturing Mg-alloy components used for numerous applications. High-pressure die casting is suitable for mass production and has the advantage of also being suitable for accurately fashioning objects of complicated shapes. One disadvantage of high-speed die casting is the occurrence of defects such as shrinkage or air entrainment. Gating system design must be very effective in actual manufacturing facilities to avoid the occurrence of such defects. The objective of this study is to present a methodology for obtaining optimal designs of 4-cavity thin electronic component housings. The fluid behavior and amount of air entrainment caused by the overflows and air vent designs were analyzed using a computer fluid dynamics (CFD) simulator. The effectiveness of the proposed system was demonstrated through CFD simulations and experiments using an actual manufacturing process. Also, the effect of vacuum systems on the porosity and mechanical properties of the castings was studied. The volume of porosity in the casting was found to be significantly reduced using vacuum assistance during die casting. As a result, the tensile strength and the elongation of the die casting products are improved.

Keywords AZ91D, die casting, mechanical properties, micro-structure, numerical simulation

1. Introduction

Kim et al. (Ref 1) and Shin et al. (Ref 2) discovered that extended magnesium alloys have the lowest density among current common alloys and can be instrumental in lowering the weight of automobiles and airplanes. Such magnesium alloys have been limited in their use due to their low ductility and corrosion resistance compared to other light materials. But with the advancement of alloy and refining technologies, the limitations that were described by the study reported (Ref 3-5) and Chang et al. (Ref 6) have been overcome. Recently, researchers (Ref 7, 8) examined the automobile industry and discovered a great interest in the applications of magnesium alloy.

Magnesium alloys with HCP structures are usually produced by casting processes for almost all their applications. Die casting is a precise casting method in which molten fluid is injected at high pressure into a die cavity. As soon as the molten fluid has filled the cavity, it solidifies by fast cooling. Die casting is widely used in the automobile, aerospace, electronics, and household appliance industries due to its results of high strength and good performance. The quality of the die cast is essentially determined by the die in which the metal is cast. The design of the gating system is very critical to the die because it will affect the subsequent design procedures and influence the overall

quality of the die cast products. Irrespective of the shape of the castings, the quality is always determined by the gating system. In general, the system contains the arrangements and shapes of gates, runners, sprues, overflows, and air vents. Herman (Ref 9) discussed the effects of the molten fluid velocity and die temperature on the molten fluid distance and quality. In the process, molten fluid is injected into the die cavity, and flows with a high velocity, commonly over 10 m/s, through gates. Brevick (Ref 10) discovered that this turbulent flow usually causes the entrapment of gas in the die cavity, and consequently induces porosities, which is a frequent reason for casting rejection. Gouraly et al. (Ref 11, 12) have greatly contributed to study on the porosity in die castings. However, the quantitative effect of porosity on mechanical properties of die castings should be studied further. In addition, the die casting paper (Ref 13-16) proposed some methods to predict gas entrapment in the mold-filling process. In spite of the study, it is well known that the die casting process is quite complicated. However, the die designer must determine the gating system used according to his own experience. This trial and error method usually results in longer lead times and increased costs for die casters.

Xiong et al. (Ref 17) used numerical methods to analyze the die casting process from a thermal perspective to shorten the costly and time-consuming lead times that are associated with process design, tool fabrication, modification, and the trial and error procedure involved in finding acceptable operating conditions. Some recent researchers studied 2-cavity molds and thin component housings at a thickness of 1 mm. But no attempts have made to study molds and component housings at a thickness of <1 mm. Also, vacuum systems have been developed for heavy housings, such as seat frames and steering wheel cores, using a computer fluid dynamics (CFD) simulator.

The main purpose of this article is to design the runner of the mold with a developed thickness of 0.3 mm and with a 4-cavity

B.D. Lee, U.H. Baek, and J.W. Han, Division of Material Science and Engineering, Inha University, Incheon 402-751, Republic of Korea. Contact e-mails: flyhigh78@gmail.com and jwhan@inha.ac.kr.

mold using a CFD simulator. Vacuum systems were analyzed for a light housing with a 4-cavity mold and a thickness of 0.3 mm. Several experiments with AZ91D die castings were carried out. The experimental results were compared with the simulated results. The porosity and mechanical properties of the specimens from the die castings were measured, and those measurements agreed well with the simulations. Also, the effect of porosity on the mechanical properties was analyzed.

2. Numerical Models

The CFD code FLOW-3D-based on a finite volume/finite difference approach was used in the simulation. Two methodologies, fractional area/volume obstacle representation (FAVOR) and volume-of-fluid (VOF), constitute the core of the software. These methods differ from methods in most other codes but offer many advantages, and are summarized in Ref 18 by Barkhudarov and Hirt.

2.1 Optimization Model Description and Simulation Condition

When using a parametric design in gating system design, the designer does not need to create the geometries of the gating system from scratch in each die design process. The main approach for developing a parametric design system is to build a gating model database and to construct adequate parametric models of gating elements using a 3D CAD tool before the gating system design is put into practice. In this case, a software package of the casting process simulation can obtain solid modeling information with a certain file format interface, such as STL. FLOW-3D software obtains solid modeling information by importing STL files from commercial 3D modeling software. Figure 1 shows the geometry and mesh setup of the

casting. In die design, runners and overflows are the important aspects for reducing the amount of trapped air. The runner and gate design was studied by Hirt and Sicilian (Ref 19). The largest percentage area reduction should occur at the gate, where an area reduction ranging from 10 to 40% is typical, as studied by Yoshimura et al. (Ref 20).

Finally, all the effort listed above is aimed at trying to force the air out of the shot sleeve ahead of the plunger, and this approach depends on having a path for the air to go. This means there must be air vents and a vacuum system. The location of the air vents is absolutely critical if the porosity is major, so the air vents should take precedence over other factors. Above all, because the object of this study is obtaining casting conditions of LCD housing with a 0.3 mm thickness, if the casting fails with the design then the casting remains in the cavity due to the quick solidification rates. Then, failure will deteriorate the quality of the casting products. Figure 1 shows additional overflow and air vents in the original model. Here, the aim of these numerical simulations was to examine the predictive capability of the model with different overflow designs and additional air vents. Different overflow designs and additional air vents have different ways of controlling the flow of molten fluid during filling. For the prevention of trapped air, a vacuum system shown in Fig. 1(d) is considered.

Jin and Kang (Ref 21) studied the location of the vacuum channel connections and discovered that they should be at the last points to fill, and this is best defined by flow simulation.

The number of cells in the mold/cavity domain is 2,981,826, with the smallest cell size being 0.2 mm from the gate to the product. Tables 1 and 2 show the physical properties and initial conditions for the simulation. SKD61 die steel was employed as a mold material at an initial temperature of 200 °C. AZ91D LCD housings were produced on a hot-chamber die casting machine. The solid and molten temperatures of AZ91D were set at 470 and 590 °C, respectively. The cross section of the

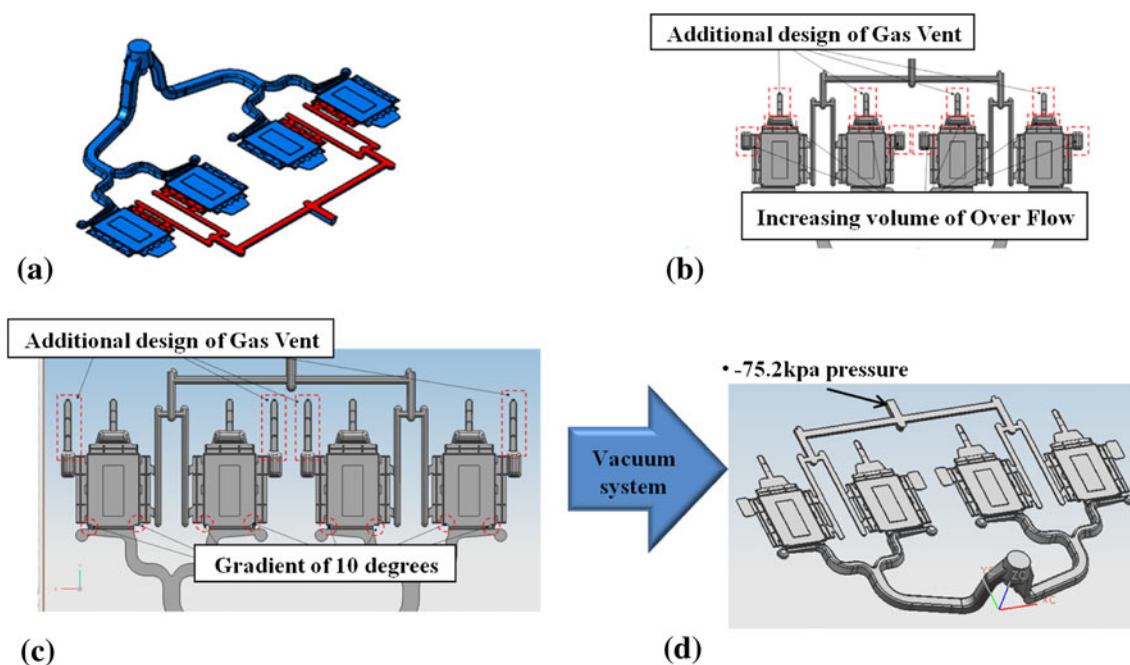


Fig. 1 Diagram of the LCD housing: (a) original model, (b) 1st corrected model, (c) 2nd corrected model, and (d) vacuum system model

Table 1 Thermo-physical properties of the casting and mold

Materials	Property	Symbol	Value	Unit
Casting (AZ91D)	Thermal conductivity of molten fluid	κ_l	72	W/(m·k)
	Thermal conductivity of solid	κ_s	254	W/(m·k)
	Specific heat of molten fluid	C_l	1050	J/(kg·k)
	Specific heat of solid	C_s	1034	J/(kg·k)
	Density of molten fluid	ρ_l	1.81	kg/m ³
	Density of solid	ρ_s	1.79	kg/m ³
	Liquidus temperature	T_l	590	°C
	Solidus temperature	T_s	470	°C
Mold (SKD61)	Thermal conductivity	κ_f	25	W/(m·k)
	Specific heat	C	0.46	J/(kg·k)

Table 2 Initial conditions for the simulation (boundary conditions)

Flow mode	Viscous fluid	Numerical approximations	Pouring temperature	Mold temperature
Incompressible	Renormalized group model	Explicit	630 °C	200 °C
Plunger velocity, 1st stage	Plunger velocity, 2nd stage	Tip diameter	Thickness (products)	Volume (products)
0.14 m/s	0.83 m/s	74 Φ	0.3 mm	3.092E+03 m ³

gate was 58.82 mm². Finally, the initial injection speeds of the plunger were 0.14 and 0.83 m/s.

2.2 Geometry Representation

An advancement of the conventional finite difference method is given by adopting the FAVOR method. In this method, rectangular grid cells can be partially blocked by obstacles (Ref 19). This improves the accuracy of the numerical solution near mold walls and allows for the use of coarser grids than in standard finite difference methods studied by Sequeira et al. (Ref 22). Since the geometry representation is less mesh-dependent, the FAVOR is also referred to as a free gridding method.

For an incompressible, viscous fluid, the FAVOR equations take the form:

$$\nabla \cdot (Au) = 0 \quad (\text{Eq 1})$$

$$\frac{\partial u}{\partial t} + \frac{1}{V}(Au \cdot \nabla)u = -\frac{1}{\rho}\nabla p + \frac{1}{\rho V}(\nabla A) \cdot (\mu \nabla)u + g \quad (\text{Eq 2})$$

$$\frac{\partial H}{\partial t} + \frac{1}{V}(Au \cdot \nabla)H = \frac{1}{\rho V}(\nabla A) \cdot (\kappa \cdot T) \quad (\text{Eq 3})$$

where

$$H = \int C(T)\partial T + L(1 - f_s) \quad (\text{Eq 4})$$

In these equations, parameters of A and u are vectors. Therefore, A is the open area fraction associated with the flow in the i th direction, V is the open volume fraction, ρ is the density, p is the pressure, u is the i th velocity component, μ is the fluid viscosity coefficient, g is gravity, H is the fluid enthalpy, T and T_m are fluid temperature and mold temperature, respectively (°C), f_s is the solid fraction, L is the latent heat, and C and κ are the fluid-specific heat and thermal conductivity coefficient, respectively. For the mold, the energy equation has the form

$$\frac{\partial T}{\partial t} = \frac{1}{\rho C_m V_c}(\nabla A_c) \cdot (\kappa_m \nabla T_m) \quad (\text{Eq 5})$$

where the subscript m indicates a parameter related to the mold and the c indicates quantities that are complements of the volume and area fractions. At the metal/mold interface, the heat flux, q , is calculated according to

$$q = h(T - T_m) \quad (\text{Eq 6})$$

where h is the heat transfer coefficient.

2.3 Evaluation of Air Entrainment

In die casting, trapped air is usually the biggest problem contributing to porosity because of the very turbulent flow and the fast fill rate that is necessary in the process. If this problem could be eliminated, die casting would probably become the prominent casting method, especially for smaller castings. In this article, the trapped air amount is estimated using a CFD simulator. Air entrainment at the molten fluid surface is based on the concept that turbulent eddies raise small molten fluid elements above the free surface that may trap air and carry it back into the molten fluid. Sequeira et al. (Ref 23) found that the molten fluid elements that can be lifted above the free surface depend on whether or not the intensity of the turbulence is enough to overcome the surface-stabilizing forces of gravity and surface tension. Turbulence transport models characterize turbulence by a specific turbulent kinetic energy Q and a dissipation function D .

The characteristic size of turbulence eddies is then given by (7).

$$L = 0.1 \frac{\sqrt{Q^3}}{D} \quad (\text{Eq 7})$$

This scale is used to characterize surface disturbances. The disturbance kinetic energy per unit volume, i.e., pressure_d (P_d) associated with a fluid element raised to a height L and with a surface tension energy based on a curvature of L is given by (8).

$$P_d = \rho g L + \sigma / L \quad (\text{Eq 8})$$

where ρ is the molten fluid density (kg/m^3), σ is the coefficient of surface tension, and g (m/s^2) is the component of gravity normal to the free surface. In addition, because the potential energy is the dominant parameter compared to the surface tension in P_d , (J), it is conceivable that the influences of surface tension are small. For air entrainment to occur, the turbulent kinetic energy per unit volume, $P_t = \rho Q$, must be larger than P_d . Said in another way, it means that the turbulent disturbances must be large enough to overcome the surface stabilizing forces. The volume of air entrained per unit time, V_a , is given as (9).

$$\frac{\partial V_a}{\partial t} + u \nabla V_a = R(1 - V_a) \quad (\text{Eq 9})$$

where $R = C_{\text{air}} \sqrt{(P_1 - P_d) / \rho}$, u is fluid velocity (m/s), t is time (s), and C_{air} is a coefficient of proportionality. In this study, $C_{\text{air}} = 0.5$, which means we assume on average that air will be trapped over about half the surface area. If P_1 is less than P_d , then V_a is zero.

The air entrainment is expressed in (10).

$$A = \sum_{k=1}^n V_{ak} F_{fk} V_{fk} V_{ck} \quad (\text{Eq 10})$$

where A is the quantity of air entrainment (in m^3), V_a is the volume of air entrained per unit time (in m^3), F_f is the fluid fraction, V_f is the volume fraction, V_c is the volume of the mesh cell (in m^3), and n is the aggregate number of mesh cells. In this study, the calculation of air entrainment is used as the measure of an evaluation studied by Dargusch et al. (24).

3. Experimental Methods

The materials used in this study were 200 tons of AZ91D alloys cast by a high pressure die casting (HPDC) process. The composition of AZ91D is shown in Table 3.

The molten fluid and solid temperatures of magnesium were about 578 and 430 °C, respectively. The vacuum system we used in the study consisted of a vacuum pump, a vacuum tank, and a vacuum valve. The 1st step for the die casting process was the molten fluid moving to the injection chamber. Second, the plunger moved past the pouring hole and sealed off the die cavity. The vacuum valve was then activated and lower-than-atmospheric pressure was created in the die cavity. The cavity was continuously evacuated from the beginning of the die filling process to the end. In the HPDC process and vacuum system, the die temperature was controlled at 200 °C. The pouring temperature was controlled at 630 °C. A variety of plunger speeds ranging from 0.14 to 0.83 m/s were used during the casting.

The tensile tests were conducted following the KS B0801 sub-size using an Instron 5569 Universal Electromechanical

Table 3 The chemical compositions of the AZ91D Mg alloy

	Al	Zn	Mn	Fe	Si	Cu	Ni	Mg
AZ91D	8.9	0.69	0.24	0.001	0.02	0.002	0.001	Bal.

Testing System equipped with Bluehill software and a 50 kN load cell. All the specimens were cut into central rectangular plates from cast products. Namely, tensile specimens were cut into perpendicular to the gas vent direction and the number of specimens was cut three from same locations. The tensile samples were tested without heat treatment. All tests were performed at ambient temperature (25 °C) and conducted at a strain rate of 10^{-3} . Dargusch et al. (24) examined the AZ91D die casting sample by XRD/SEM and identified it to have an $\alpha + \beta$ dual-phase microstructure. Specimens for microstructural characterization were cut from the middle section of the die casting samples. The microstructure of the HPDC and vacuum system samples was examined by optical microscopy (OM) with quantitative metallography. The specimens for OM were prepared by the standard technique of grinding with SiC abrasive paper and polishing, followed by etching in an aqueous solution of 60 vol.% ethylene glycol, 20 vol.% acetic acid, and 1 vol.% concentrated HNO_3 . For the determination of the quality of the die casting samples, two distinct criteria were used. In the first one, the visual inspection of the amount of porosity was analyzed by computed tomography (CT). CT is a non-destructive evaluation technique for visualizing and inspecting the internal structure of objects.

After completing the CT data acquisition and reconstruction process, we have a 3D volumetric density distribution of the object. Using visualization tools we can view the object from different perspectives. We can rotate the object, zoom into an area of interest, slice the object at any orientation (arbitrary sectioning), and measure density, distance, area, and volume. The data acquisition process also provides a complete set of digital radioscopic images that can be used for further analysis. The second criterion that we used was a density determination of the machined part using Archimedes' principle.

4. Results and Discussion

4.1 Numerical Simulation

When molten fluid is injected under high pressure into the die cavity, the entrapment of gas by these flows during metal filling is one of the primary causes of porosity. Unless we design an appropriate molten fluid velocity and die temperature, the gases evolved during mold filling may float through the casting and leave oxide trails. These defects are difficult to control and may not be found until castings are cleaned, machined, and inspected. However, the simulation of the filling process takes a virtual look inside the die, sees exactly how defects are being generated, and gives us information about the possible problems.

In the study, for reducing the trapped air in the die casting process, it is important to observe the fluid flow of magnesium melt. The first study involved the prediction of the filling behavior of an LCD 4-cavity housing. It was about 300×300 mm in area and had a section thickness of 0.3 mm. The filling parameters used in the simulation were: pouring temperature, 630 °C; preheated temperature of the mold, 200 °C; 1st plunger speed in the ingate, 0.14 m/s; 2nd plunger speed in the ingate, 0.83 m/s. The process parameters used in Fig. 2(a) are the same as those used in Fig. 2(b) to (d). Figure 2 shows the mold-filling simulation results of the HPDC AZ91D magnesium alloy in the cavity of the LCD housing. Molten fluid enters the die cavity through four gates attached to

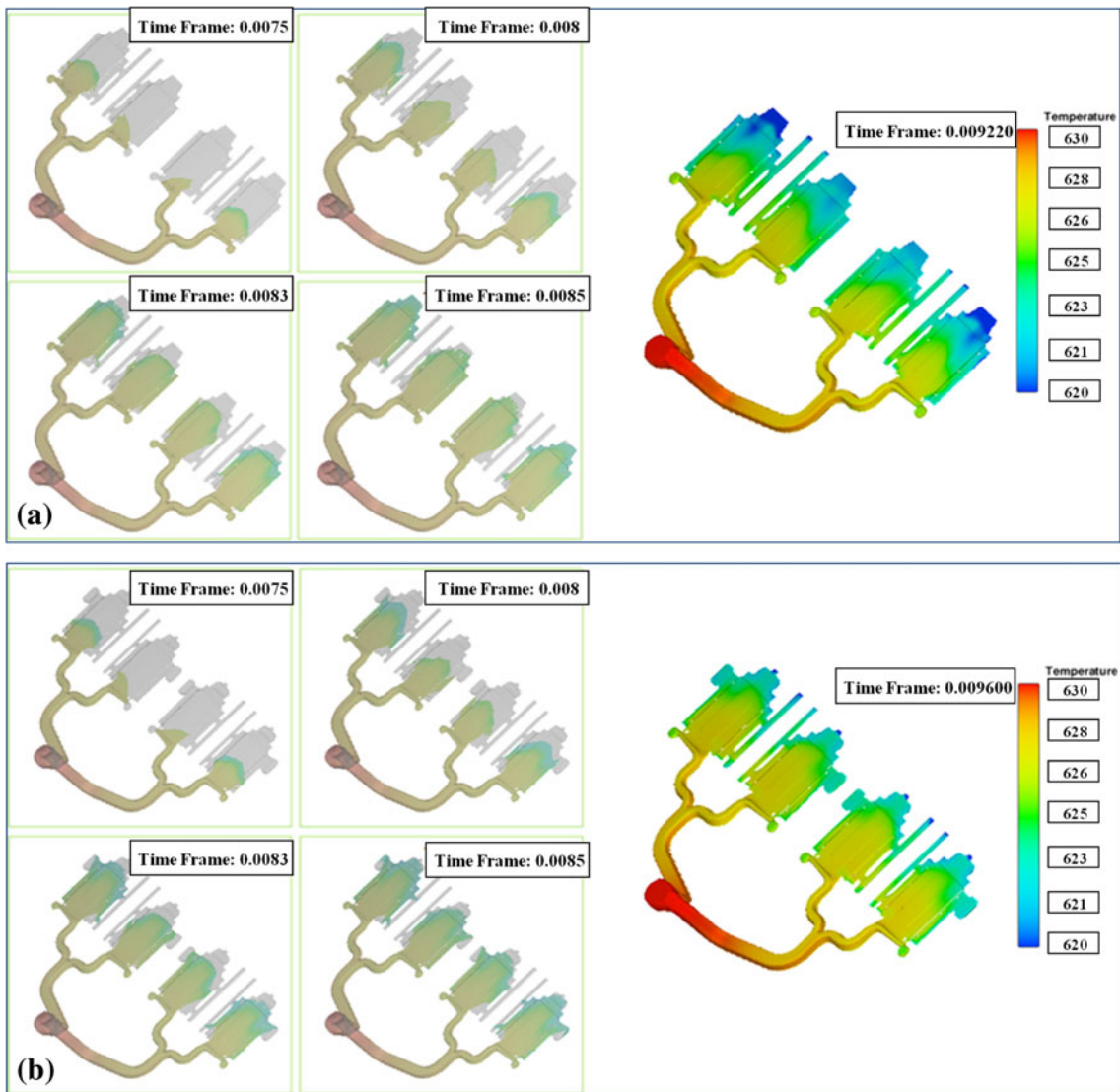


Fig. 2 The filling sequences of numerical simulation for: (a) original model, (b) 1st corrected model, (c) 2nd corrected model, and (d) vacuum system model

the Y-shaped runner. It can be seen from Fig. 2 that the filling process is stable in all filling stages. The molten fluid flows through the runners at first and fills the gates preferably.

Finally, the cavity of the LCD housing was filled by molten fluid, as shown in Fig. 2(a). But the filling velocity in the cavity was slower than the velocity in the center because of the fast cooling and great resistance in both sides of the cavity. The filling velocity in the 2nd and 3rd cavities was 0.075 m/s faster than the velocity in the center. In this case, we predicted that the flow of unstable molten fluid will increase the amount of trapped air in the 2nd and 3rd cavities. The transition from yellow to green shows where the incoming fluid decelerates as it encounters the back filling fluid which moves more slowly. The high temperature follow-up fluid remelted the leading low temperature fluid. The molten fluid substantially filled the cavity above about 80% at a rate of 0.008 m/s.

This is thought to result from the different molten fluid velocity, where the 1st plunger speed turned into the 2nd plunger speed. Some molten fluid was discharged from the overflow at the top of the cavity. Because the air vents are very

narrow and comparable to the overflow thickness, the discharge of molten fluid through the air vents on both sides occurs late in the filling.

It can be seen from Fig. 2(a) that molten fluid is still stable and the filling character is analogous to that in Fig. 2(b) to (d). But the molten fluid has completely filled the cavity and the entire temperature distribution is different. We predicted the effect of overflows and an additional air venting system. This is thought to result from the comparability of the filling rate, as shown in Fig. 3. When the filling volume reaches about 90% (see Fig. 3 at $9.03\text{E}-03$ s), the fluid of the original model began to decelerate sharply as it approached the overflow on the top of the cavity. Though the fluid of the corrected model is somewhat stable, the fluid at $9.03\text{E}-03$ s was delayed for a bit. However, the fluids of the 2nd corrected model and vacuum system model resulted in a stable filling rate based on the numerical simulation. In the study, the simulation results in Fig. 2 and 3 are in good agreement. The simulation results in Fig. 2 indicate that it is important to design overflows and air vents. Even though the system change with respect to overflow

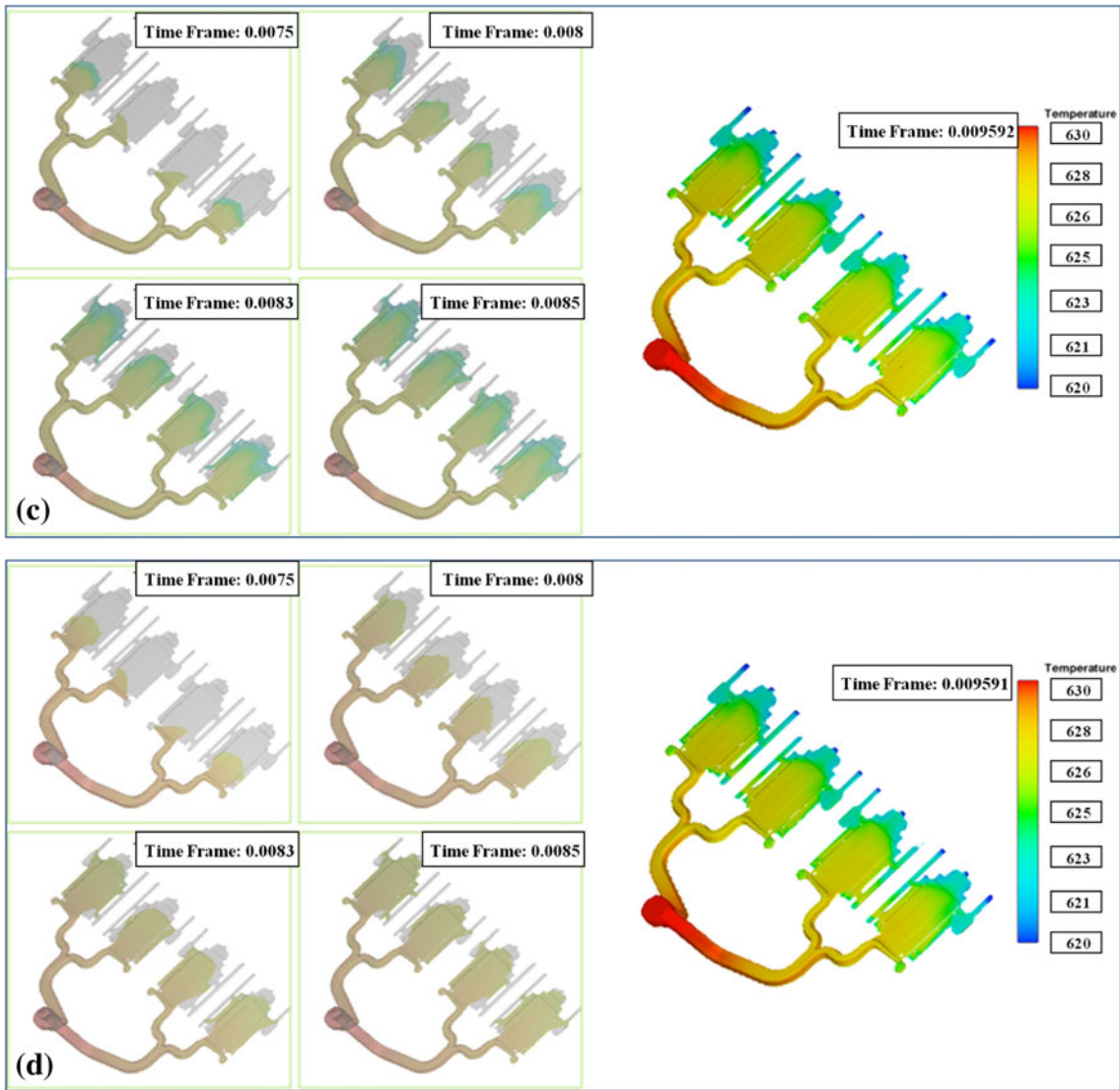


Fig. 2 Continued

and air vents affected the product of the temperature distribution, the model did not appear to exhibit any difference in the temperature distribution.

We designed a model based on the porosity interpretation to study the vacuum system in detail.

The molten fluid simulations considering air entrainment were performed, and the influence of the overflow, air vent, and vacuum systems was investigated. The calculated results for the amount of air entrainment are contained in Fig. 4. The entrained air was greatly reduced. After complete filling, the total amount of air entrainment for the simulation results was 0.952, 0.892, 0.602, and 0.534 for the cases in Fig. 4(a), (b), (c), and (d), respectively. The amount of air at the red circle had simulated values of 0.32, 0.021, 0.018, and 0.004, respectively. The 2nd corrected model had 58% lower values compared to the original. Moreover, the vacuum system model showed enhanced results compared to the 2nd corrected model by 13%. As a result, the result using the vacuum system model was 78% lower than that of the original design. Though the vacuum

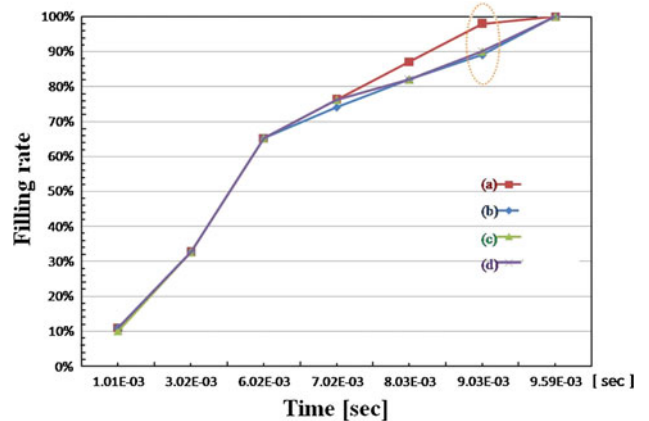


Fig. 3 Filling rate of numerical simulation for: (a) original model, (b) 1st corrected model, (c) 2nd corrected model, and (d) vacuum system model

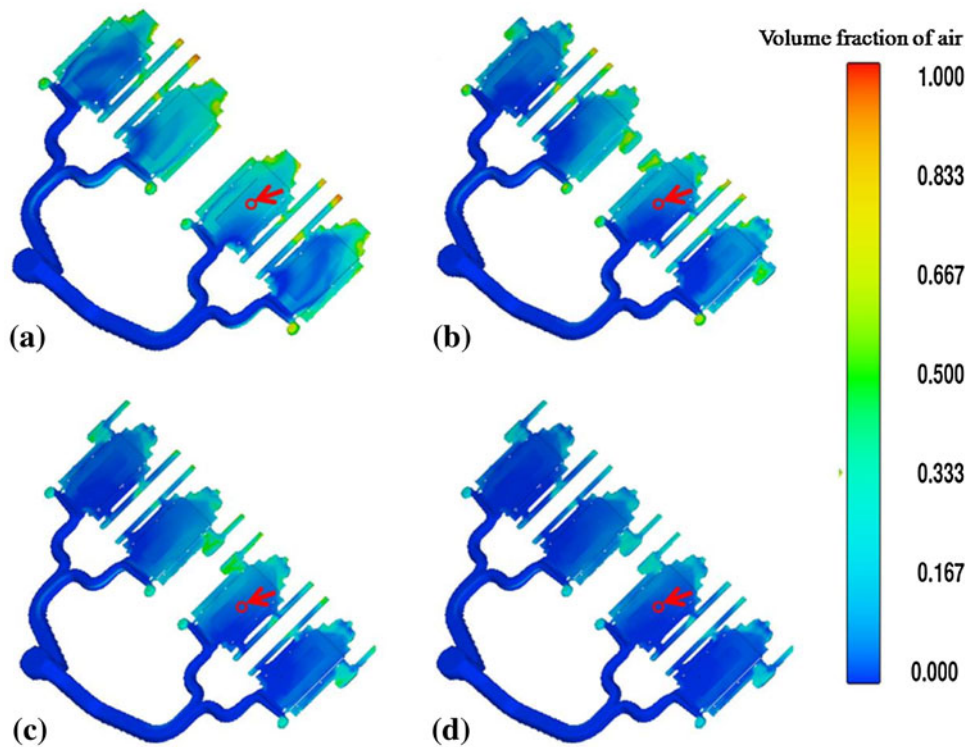


Fig. 4 Volume fraction analysis of air for: (a) original model, (b) 1st corrected model, (c) 2nd corrected model, and (d) vacuum system model

system of the 0.3 mm thin product did not affect the temperature distribution, it was found to be very efficient for removing porosity in the cavity with a vacuum system. Thus, by optimizing the design of the overflow with an air vent with vacuum systems, a decrease in the amount of air was achieved. As a result, we could conclude that the original process was unsuitable for this casting, while the corrected model process (1st corrected model and 2nd corrected model) will lead to better results.

4.2 Experimental Validation

There are several physical processes influencing volume shrinkage during solidification. Because molten fluid is nearly incompressible, any loss in volume caused by shrinkage must be replaced by new molten fluid or by the opening of a void somewhere in the casting. After molten fluid has cooled enough for its solid fraction to exceed the point of rigidity, there can be no (or very little) additional molten fluid flow to compensate for the shrinkage. Figure 5 shows the location of samples taken and CT results used for analyzing internal defects. There were more micropores and the pores were somewhat larger in the center of the samples than at the sample surfaces. This is in accordance with the porosity evaluation in the literature published by ASM (25). But, the internal defects in the study showed a combination of shrink and air porosity at the overflow, as in Fig. 5. It can be seen from Fig. 5(a) that the internal defects are analogous to those in Fig. 5(b) to and (d). The reason being was that it was difficult for the CT method to analyze the internal defects with sizes below 60 μm . The LCD housing has a small defect size because it solidified quickly and the casting has a thickness of < 1 mm. For a better analysis of the 0.3 mm thick components, an additional method, such as Archimedes's principle, needs to be considered.

Figure 6 shows the result from using Archimedes's principle. The porosity ratio of the 2nd corrected model decreased by 40% compared to the original model. It is similar to the result of the simulation.

Figure 7 compares the simulation and the experimental results with respect to the decreased ratio of porosity. Even though the result of the experiment data was only a little different compared to the simulation, it has a tendency to have a lower porosity in the cavity with the vacuum system.

A tensile test to analyze the effect of porosity on the mechanical properties in the cavity was performed. Figure 6(c) shows the results of the mechanical test in the LCD housing. The tensile strength is 291, 309, 326, and 335 MPa for the respective models in the figure. Among the four investigated models, the vacuum system model exhibits the most significant improvement in tensile strength and elongation by vacuum assistance. The reason being is that porosity affects the fracture of specimens. The mechanical properties of an alloy depend on the defects that may be present in the matrix. These defects could be point, line, surface, or volume defects. Among these defects, volume defects (porosity, secondary phases, or inclusions) are known to be the most significant ones and may dramatically affect the mechanical properties. The size and volume of these defects are critical since they act as the initiation points for porosity and also as stress risers, as examined by Nave et al. (26).

It is obvious that there is a lot of porosity in the low tensile strength model. These porosities induce stress concentration and crack initialization, which result in quite poor tensile strength and the elongation of samples. It is well known that in the presence of defects or stress risers the components may fracture at stresses far away from their nominal theoretical limits. Figure 6(b) and (c) is perfect examples of such phenomena. Also, the yield strength of Mg alloys fabricated

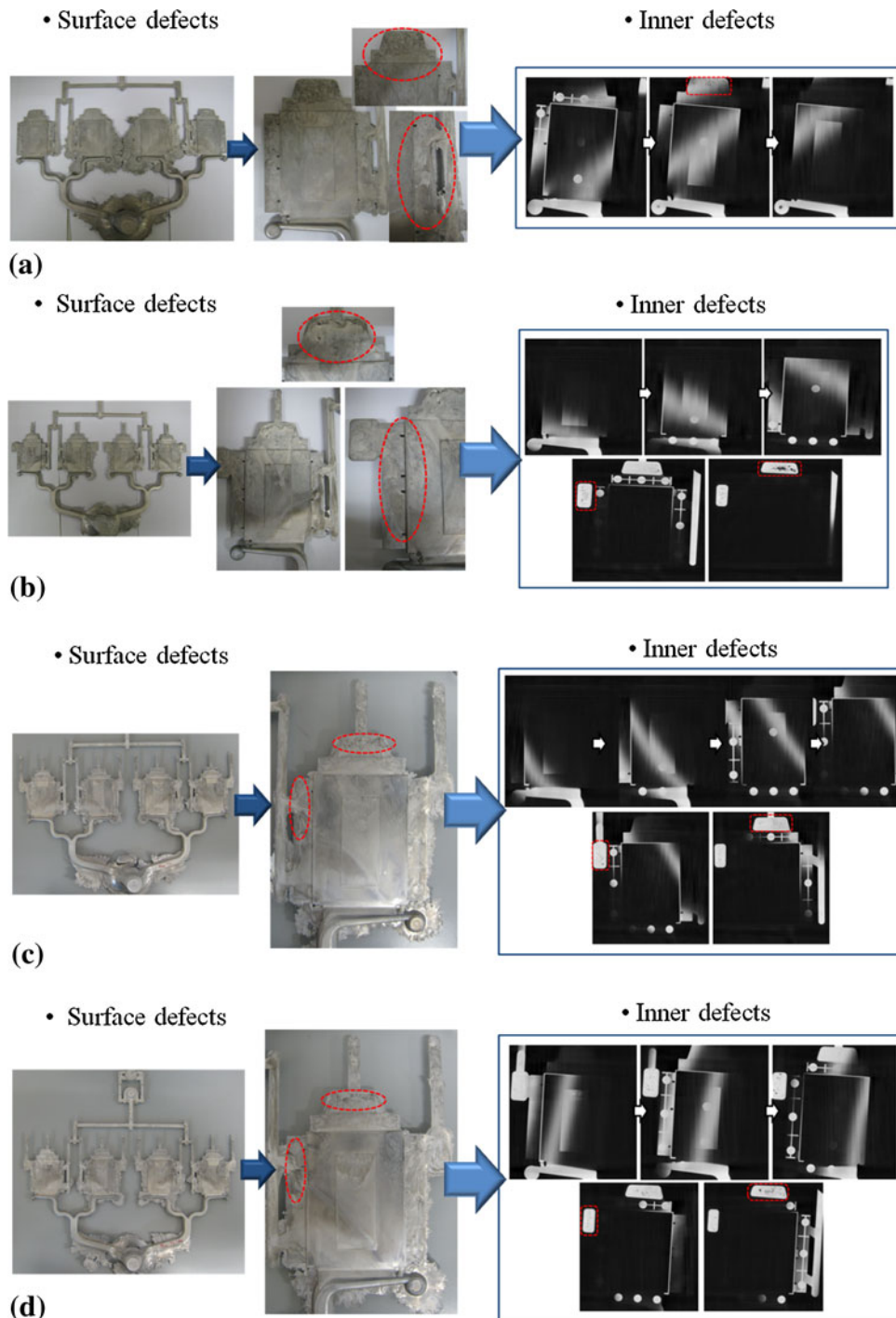


Fig. 5 Location of samples taken and CT analysis results of the distribution of internal defects in the LCD housing: (a) original model, (b) 1st corrected model, (c) 2nd corrected model, and (d) vacuum system model

by the die casting method was influenced by other factors, such as the mean size of grains and precipitates of the $Mg_{17}Al_{12}$ phase. The reason, as given in Fig. 8(a) and (c), illustrated that grain size influenced the yield strength, and the 2nd corrected model had maximum yield strength of about 259 MPa among all specimens.

Figure 7(a) shows the microstructural change in the LCD housing as a function of the gating system. The grain size at the gating systems and vacuum systems is 8.13, 7.16, 7.92, and

8.20 μm for the respective models given in the figure. The grain size from the 1st and 2nd corrected models is more refined than that of the original and vacuum system models. This result was slightly different from the die casting process. In the study, the grain size is not important because we focused on the entrapped air.

Cracks are easily formed in the porosity of conventional die castings, because of the high stress concentration due to the reduced effective area.

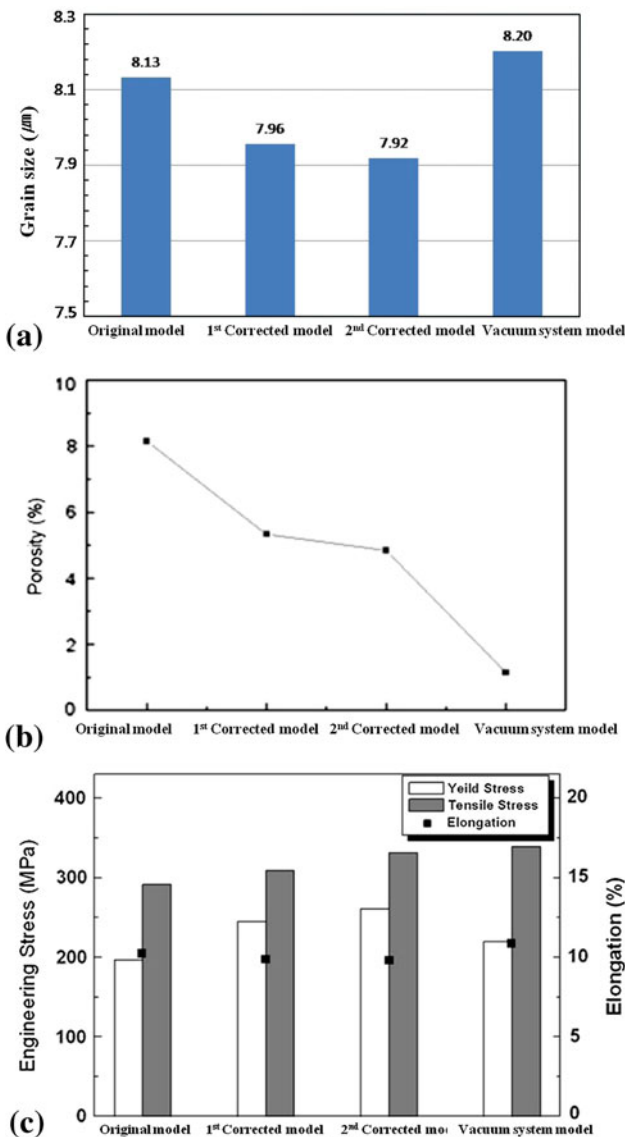


Fig. 6 Experimental data of LCD housing: (a) grain size, (b) porosity with a different gate design, and (c) mechanical properties

The microstructure and fracture of tensile test of the HPDC alloy are illustrated in Fig. 8. Generally speaking, Chen et al. (27) showed that the extended Mg alloys consist of an Mg-rich phase with a β phase located at the grain boundary. Figure 8 shows the typical microstructure of the permanent mold cast AZ91 alloy.

Nave et al. (28) discovered that the alloy consists of a solid α -Mg solution containing Al, Zn, and the divorced eutectic consists of a massive $Mg_{17}Al_{12}$ phase and a supersaturated Mg solid solution. Discontinuous precipitates of $Mg_{17}Al_{12}$ are also observed in the vicinity of the massive eutectic. Dorum et al. (29) studied the presence of zinc and discovered that a comparatively faster cooling process in a permanent mold produces a divorced eutectic.

The thickness of the products at the start and end of die casting must be unchanged. This study was focused on a 0.3 mm thin product even though the deviation of the product

took place due to surface defects, such as the inner porosity and heterogeneous solidification contraction. Finally, the precedence of injecting molten fluid with air entrainment and oxide concentration improves the flow fluid with a vacuum system. Therefore, the improved flow fluid reduces surface and inner defects because molten fluid quickly flows out of the overflows and air vents before solidification. Also, the fast solidification affects the efficiency improvement of the process. Figure 9 shows the results of the produced surface of the LCD housing by the adaptive vacuum system.

The trial results indicate that the LCD housing of the vacuum system has a very good surface finish throughout the entire casting.

5. Conclusions

In this study, we investigated the effect of different casting designs and vacuum systems while casting 0.3 mm thick LCD housings. The main conclusions of this study are summarized below:

- (1) The simulation results of cavity filling and air entrapment confirmed the validity of the simulation analysis.
- (2) The simulations that considered air entrainment were performed and the influence of the gating system and vacuum system were investigated.
- (3) We compared the gating system with a filling behavior and the porosity rate analyses in the cavity and optimum process conditions adapted for the die casting. The results of the model show good agreement with the available experimental data.
- (4) In the result of the simulation, surface defects and inner defects of the casting products had satisfactory results in the model that had overflow and air vents at the points of difficult filling behavior. A special T_2 model was the best model. There were almost no defect differences between the T_2 model and the T_2 vacuum model based on surface defect and inner defect analyses. This result agreed with the conclusions of the analysis.
- (5) However, the results of the analysis of the porosity rate using Archimedes' principle, which can detect defects under 60 μ m, were quite different. It was the same as the results from the simulation interpretation. Finally, the specimens of the T_2 vacuum model indicated that the vacuum-assisted die casting process resulted in a reduced porosity when compared to the T_0 , T_1 , and T_2 models.
- (6) Also, we performed tensile testing to analyze the effect of inner defects on mechanical properties of LCD housings. Mechanical properties of LCD housings increase with less porosity rates. The porosity of specimens influences the tensile strength and elongation and the T_2 vacuum model had improved mechanical properties.
- (7) The result of the casting products from the adapted vacuum system using a thick deviation was satisfactory without inner defects and solidification contraction. Also, we developed good products for 4-cavity LCD housings that were 0.3 mm in thickness.

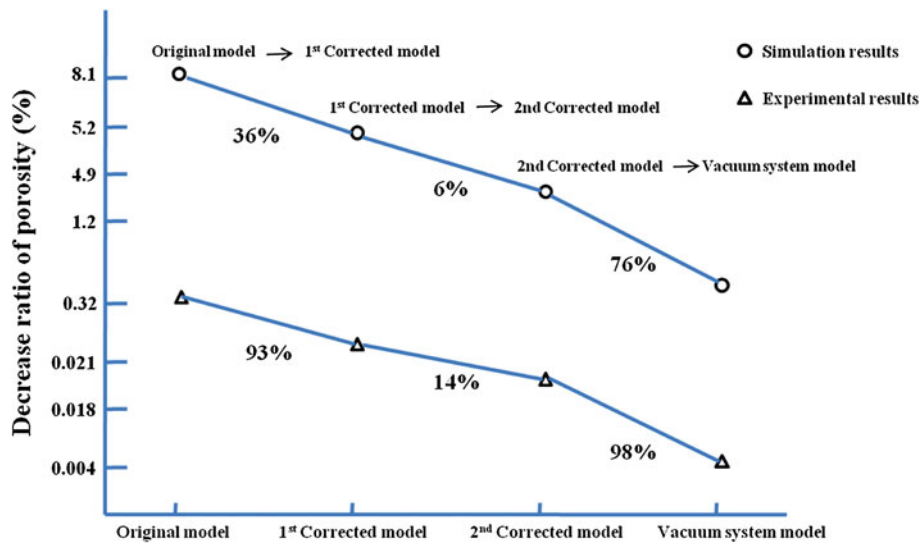


Fig. 7 Comparison of simulation and experimental results of the decreased ratio of porosity

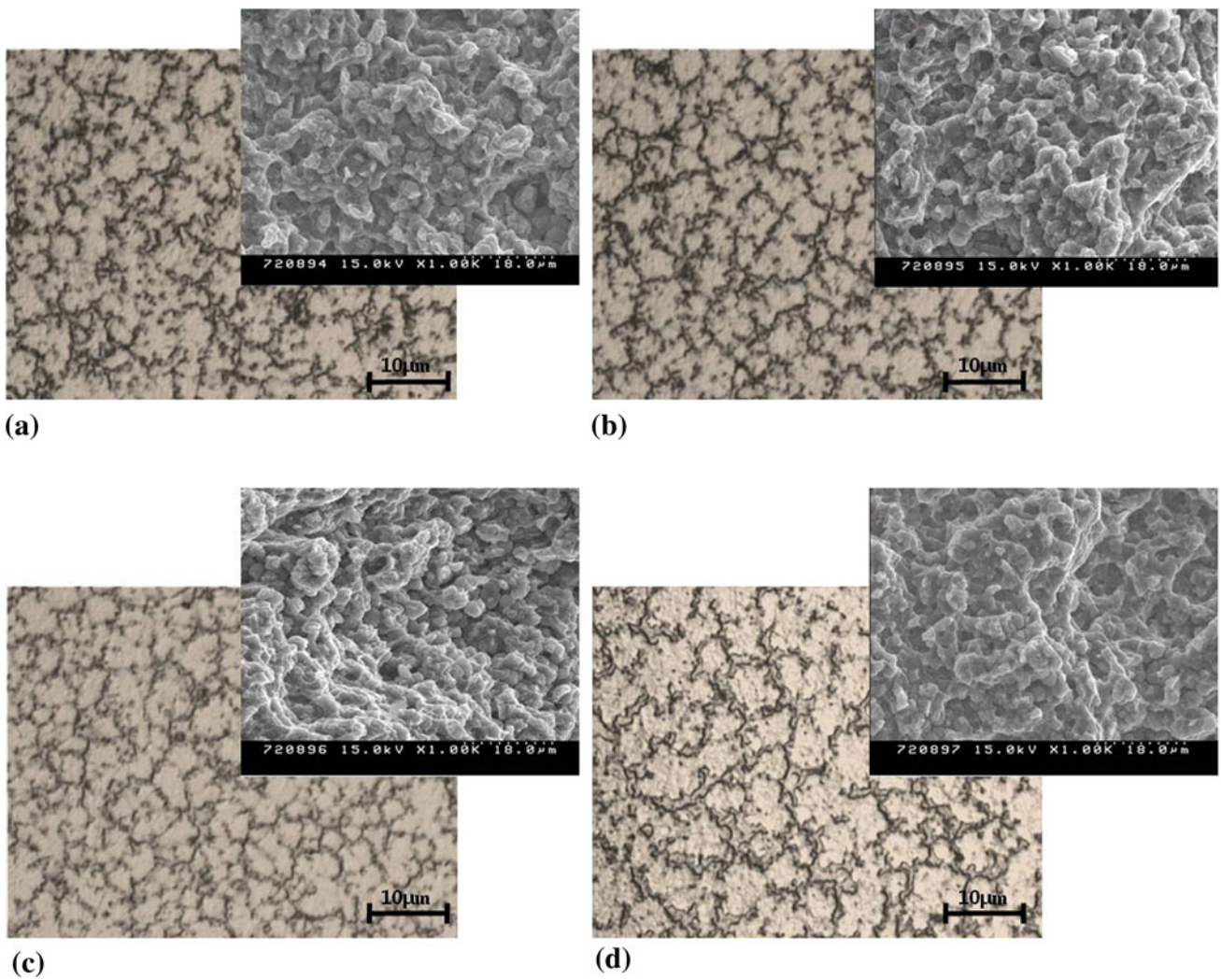


Fig. 8 Microstructure of LCD housing by die casting process: (a) original model, (b) 1st corrected model, (c) 2nd corrected model, and (d) vacuum system model

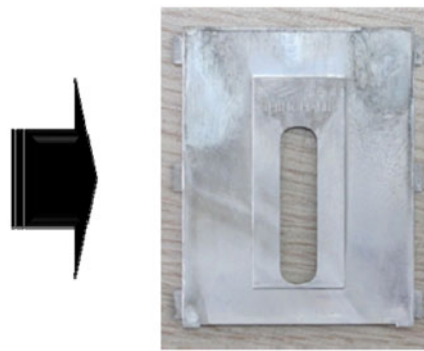
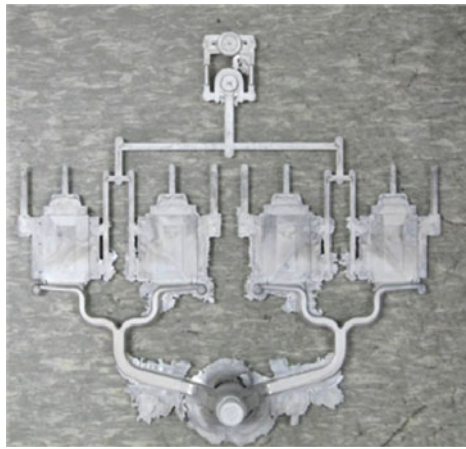


Fig. 9 Produced 0.3 mm thickness LCD housing by vacuum system

Acknowledgments

This research was supported by a grant from the Materials & Components Technology R&D Program Funded by The Ministry of Commerce, Industry and Energy, Republic of Korea.

References

1. S.K. Kim, J.K. Lee, Y.O. Yoon, and H.H. Jo, Development of AZ31 Mg Alloy Wrought Process Route, Without Protective Gas, *J. Mater. Process. Technol.*, 2007, **187–188**, p 757–760
2. B.S. Shin, Y. Kim, and D.H. Bae, Deformation Behavior of a Wrought Mg-Zn-RE Alloy at the Elevated Temperatures, *J. Korean Inst. Met. & Mater.*, 2008, **46**, p 1–5
3. A. Luo, J. Renaud, I. Nakatsugawa, and J. Plourde, Magnesium Castings for Automotive Applications, *J Manag.*, 1995, **47**, p 28–31
4. D.M. Magers, *Light Materials for Transportation Systems*, Vol 53, Center for Advanced Aerospace Materials POSTECH, Pohang, 1993
5. O. Lunder, T.Kr. Aune, and K. Nisanciogtu, Effect of Mn Additions on the Corrosion Behaviour of Mould-Cast Magnesium ASTM AZ91, *Corrosion*, 1987, **43**, p 291
6. S.Y. Chang, D.H. Lee, B.S. Kim, T.S. Kim, Y.S. Song, S.H. Kim, and C.B. Lee, Characteristics of Plasma Electrolytic Oxide Coatings on Mg-Al-Zn Alloy Prepared by Powder Metallurgy, *Met. Mater. Inst.*, 2009, **15**, p 759–764
7. B.S. Shin, J.W. Kwon, and D.H. Bae, Microstructure and Deformation Behavior of a Mg-RE-Zn-Al Alloy Reinforced with the Network of a Mg-RE Phase, *Met. Mater. Inst.*, 2009, **15**, p 203–207
8. S.H. Choi, D.H. Kim, and B.S. Seong, Simulation of Strain-Softening Behaviors in an AZ31 Mg Alloy Showing Distinct Twin-Induced Reorientation Before a Peak, *Met. Mater. Inst.*, 2009, **15**, p 239–248
9. E.A. Herman, *Die Casting Dies: Design*, North American Die-casting Association, 1992, p 15–24
10. J.R. Brevick, Die Casting Defects Causing Rejections During Machining, *Die Cast. Eng.*, 1997, **5**, p 42–46
11. C.M. Gourlay, H.I. Laukli, and A.K. Dahle, Defect Band Characteristics in Mg-Al, Al-Si High-Pressure Die Castings, *Metall. Mater. Trans. A*, 2007, **38A**, p 1833–1844
12. S.G. Lee and A.m. Gokhale, Formation of Gas Induced Shrinkage Porosity in Mg-Alloy High-Pressure Die Castings, *Scripta Mater.*, 2006, **55(4)**, p 387–390
13. M. McLaughlin, C.W. Kim, and A. Conrad, Flow Pattern in the Casting Process, *Mater. Des.*, 2004, **25**, p 655–661
14. A. Kimatsuka, I. Ohnaka, J.D. Zhu, and T. Kamitsu, Mold Filling Simulation with Consideration of Gas Escape Through Sand Mold, *Int. J. Cast. Met. Res.*, 2002, **15(3)**, p 149–152
15. A. Kimatsuka, I. Ohnaka, J.D. Zhu, and T. Omichi, Mold filling simulation of high pressure die casting for predicting gas porosity, *Model. Cast. Weld. Adv. Solidif. Process.* 2003, p 335–342
16. T. Sakuragi, Prediction of Gas Hole by Mold-Filling Simulation with Consideration of Surface Tension, *JSME Int. J. B*, 2004, **47(4)**, p 699–708
17. S.M. Xiong, F. Lau, and W.B. Lee, Numerical Methods to Improve the Computational Efficiency of Thermal Analysis for the Die Casting Process, *J. Mater. Process. Technol.*, 2002, **128(1–3)**, p 19–24
18. M.R. Barkhudarov and C.W. Hirt, *Casting Simulation: Mold Filling and Solidification—Benchmark Calculations Using FLOW-3D®*, Technical Report, Flow Science, Inc., Santa Fe, 1993
19. C.W. Hirt and J.M. Sicilian, *Proceedings of the 4th International Conference on ShiHydrodynamics*, Washington, DC, September 1985
20. T. Yoshimura, K. Yano, T. Fukui, S. Yamamoto, S. Nishido, M. Watanabe, and Y. Nemoto, Optimum Design of Die Casting Plunger Tip Considering Air Entrainment, *Proceedings of 10th Asian Foundry Congress (AFC10)*, Nagoya, Japan, May 2008 20
21. C.K. Jin and C.G. Kang, Fabrication Process Analysis and Experimental Verification for Aluminum Bipolar Plates in Fuel Cells by Vacuum Die-Casting, *J. Power Sources*, 2011, **196**, p 8241–8249
22. W.P. Sequeira and G. L. Dunlop, Effect of Section Thickness and Microstructure on the Mechanical Properties of High Pressure Die Cast Magnesium Alloy AZ91D, 3rd International Magnesium Conference, Institute of Materials (UK), Manchester, England, 10–12 April 1996, p 63–73
23. W.P. Sequeira, M.T. Murray, G.L. Dunlop, and D.H. StJohn, Effect of Section Thickness and Gate Velocity on the Microstructure and Mechanical Properties of High Pressure Die Cast Magnesium Alloy AZ91, Automotive Alloys, A Special symposium, TMS Annual Meeting and Exhibition, Orlando, Florida, USA, February 9–13, 1997
24. M.S. Dargusch, G.L. Dunlop, and K. Pettersen, *Proc. Magnesium Alloys and Their Application*, Wolfsburg, B.L. Mordike and K.V. Kainer, Eds., Warkstoff-Informationsgesellschaft mbh., Frankfurt, 1998, p 82–277
25. ASM Handbook Committee: *Metallography and Microstructures*, ASM International, Metals Park, OH, 1985, p 425–434
26. M. Nave, A.K. Dahle, and D.H. St John, The Effect of Solidification Rate on the structure of Magnesium-Aluminium Eutectic Grains, *Int. J. Cast Met. Res.*, 2000, **13**, p 1–7
27. Y. Chen, Q. Wang, J. Peng, C. Zhai, and W. Ding, Effects of Extrusion Ratio on the Microstructure and Mechanical Properties of AZ31 Mg Alloy, *J. Mater. Process. Technol.*, 2007, **117**, p 281–285
28. M.D. Nave, A.K. Dahle, and D.H. St John, *TMS Annual Meeting*, Nashville, TN, H.I. Kaplan, J.N. Hryn, and B.B. Clow, Eds., TMS, Warrendale, PA, March 2000, p 233–242
29. C. Dørum, O.S. Hopperstad, T. Berstad, and D. Dispinar, Numerical Modeling of Magnesium Die-Castings Using Stochastic Fracture Parameters, *Eng. Fract. Mech.*, 2009, **76**, p 2232–2248